



Experimental study of corroded RC beams: dissipation and equivalent viscous damping ratio identification

C. Lejouad · B. Richard · P. Mongabure · S. Capdevielle · F. Ragueneau

Received: 19 September 2020 / Accepted: 5 February 2022 / Published online: 25 February 2022
© RILEM 2022

Abstract Corrosion of steel reinforcement is one of the most common durability issues for reinforced concrete (RC) structures, especially when located in marine areas. The study of the mechanical consequences of this pathology is of great importance to assess their performance. Experimental campaigns have been carried out on corroded structures. So far, assessing quasi-static behavior or predicting the dynamic response of structures have been based exclusively on quasi-static loadings. In particular, the dissipated energy and the damping capacity, which

are important features to study when assessing the seismic performance of corroded RC members, are evaluated based on quasi-static loadings. The objective of this study is to characterize these two significant engineering demand parameters (EDP) using both quasi-static and dynamic tests. To reach this goal, an experimental campaign is conducted on large-scale RC beams. The corroded and non-corroded RC beams are subjected to a four-point bending loading and to dynamic loading keeping the same loadings and boundary conditions. The dynamic loading is applied on the specimen by means of the AZALEE shaking table. In this paper, a brief description of the experimental campaign is made. Then, results showing the influence of the corrosion rate on the dissipation capacity of RC structures are exposed. Especially, the consistency between quasi-static and dynamic results is assessed and discussed.

C. Lejouad · P. Mongabure
Atomic Energy and Alternative Energies Commission,
CEA, D36, F-91191 Gif-sur-Yvette, France
e-mail: chaymaa.lejouad@gmail.com

P. Mongabure
e-mail: philippe.mongabure@cea.fr

B. Richard (✉)
French Institute for Radioprotection and Nuclear Safety,
IRSN, 31 avenue de la Division Leclerc,
F-92260 Fontenay-aux-Roses, France
e-mail: benjamin.richard@irsn.fr

S. Capdevielle
Université Grenoble Alpes, CNRS, 621 Avenue Centrale,
F-38400 Saint-Martin-d'Hères, France
e-mail: sophie.capdevielle@univ-grenoble-alpes.fr

F. Ragueneau
LMT, ENS Paris-Saclay, CNRS, Université Paris-Saclay,
61 Avenue du Président Wilson, F-94235 Cachan, France
e-mail: frederic.ragueneau@ens-paris-saclay.fr

Keywords Steel corrosion · Shaking table · Reinforced concrete · Dissipation · Damping

1 Introduction

Corrosion of steel reinforcement is one of the most widespread pathologies that leads to a loss of structural performance of reinforced concrete (RC) components. This statement is particularly true for RC



structures located in marine areas with exposure to chloride ions and humidity.

At the material scale, the corrosion consequences are numerous: reduction of the steel reinforcement cross-section and ductility [1], concrete cover cracking [2] and bond strength variation between steel and concrete [3].

Corrosion degradation leads to structural modifications at the member scale. In order to assess these effects, several experimental campaigns have been conducted. These experimental programs considered specimens of various types and dimensions, from small scale RC beams [4] to large scale RC columns [5–8].

The experimental campaigns carried out so far have investigated the effect of steel reinforcement corrosion on the quasi-static behavior of RC structures using either monotonous [7, 9] or cyclic loadings [10, 11]. Based on the experimental results, a decrease of the static properties, namely the bearing capacity, the ductility and the stiffness with an increasing corrosion ratio has been observed.

Several coastal regions are located in seismic zones such as in Italy [12]. For this reason, the study of the dynamic behavior of corroded RC structures is of crucial importance. The energy dissipation capacity is an important indicator when studying the seismic behavior of RC structures. It quantifies the ability of a structure to accommodate the seismic demand and therefore, to dissipate energy without compromising the structural stability, especially regarding safety. The equivalent viscous damping ratio (EVDR), which characterizes the dissipation due to the non-linear (hysteretic) behavior, provides knowledge about the seismic response of RC elements. In common practice, the EVDR is deduced from the quasi-static cyclic response [10, 11] using Jacobsen's area method [13].

Few experimental campaigns using dynamic loadings have been performed. Among them, an experimental campaign was carried out by [14] on corroded RC frames in order to assess the influence of corrosion on the modal properties of RC structures. Using hammer shock tests, an increase in the modal damping ratio is observed for an increasing corrosion degree. However, at a critical corrosion degree, this quantity of interest tends to decrease. Contradictory results were obtained in another study [15], in which the authors observed a decrease of the damping ratio for the corroded specimens. Based upon this observation,

there is no consensus in the literature on the effect of corrosion on the damping capability of RC structures and additional studies should be performed to clarify this issue. In [16], shaking table tests were performed on corroded bridge piers. An increase in the damping ratio have been observed as the corrosion gravity gets worst. From this brief literature review, it is indicated that there are no universal agreements on the effect of reinforcement corrosion on the damping capacity of RC structures. Hence, more experimental investigations are required to address the inconsistency between these different results.

Some studies on RC structures have identified these important parameters relying on both the quasi-static cyclic and the dynamic response [14] keeping the same experimental setup. The non-parametric identification method is [17] used in this type of studies to evaluate the dissipation capacity. According to the authors' knowledge, no similar experimental study has been performed on corroded RC structures.

Experimental campaigns using cyclic loadings are a significant means to predict the dynamic response of structures. However the inertial effect is not taken into account in such experiments. Furthermore, if viscous effects are introduced, they cannot be considered in such type of tests. For these reasons, an experimental campaign has been carried out on 18 large-scale corroded RC beams, in addition to two non-corroded RC beams. The corroded beams are subjected to a cyclic four-point bending loading as well as to dynamic loadings using a shaking table and using the same experimental setup. This study aims to:

- (1) Provide numerical models with some input data regarding the dissipation capacity of corroded RC components;
- (2) Compare the trends of specific structural properties (eigenfrequency, damping ratio) identified from quasi-static and dynamic responses;
- (3) Compare different identification methods to estimate damping based on quasi-static and dynamic experimental results.

This paper will first give an overview of the experimental campaign carried out. Then, the experimental results in terms of dissipation and damping capacity, obtained from quasi-static as well as dynamic testing, are underlined. Finally, the



concordance between the results of dynamic and quasi-static testing is evaluated.

2 Experimental campaign

2.1 Scope

The experimental campaign DYSBAC, a French acronym for “Dynamic behavior of corroded RC structures”, is performed by means of the AZALEE shaking table and the strong floor, which are parts of the TAMARIS experimental facility operated by the French Alternative Energies and Atomic Energy Commission (CEA) located in Saclay, France. The main objective of this experimental campaign is to study the influence of corrosion on the dynamic behavior of RC beams. In particular, the energy dissipation and the damping capacities are evaluated based on the results acquired from both quasi-static and dynamic tests. Thereafter, the results are cross-checked in order to assess the consistency between the two types of identifications.

2.2 Specimen details

In order to be representative of real RC structures and overcome any scale effect, the choice of large-scale RC beams has been made. Each beam is 4.5 m long with a cross-section of $20 \times 40\text{cm}^2$.

The reinforcement pattern is designed according to the European standards Eurocodes 2 and 8 [18, 19]. The steel reinforcement consists of ribbed B500A steel bars according to the French steel classification NF A 35-080-1 [20]. 4 bars of 12mm diameter constitute the longitudinal reinforcements and the transversal reinforcement is formed of 8mm diameter stirrups with a spacing of 10cm. The concrete cover thickness is 3cm.

The 20 specimens are cast with a C25/30 concrete class according to the Eurocodes 2 [18]. The considered concrete is formulated with a high water cement ratio of 0.59. This leads to a porous and low strength concrete, representative of concrete in aged RC structures.

2.3 Accelerated corrosion of the specimens

Since using natural corrosion process to obtain corroded specimens is highly time-demanding [9], some technics are used in order to reduce the required time exposure [21–25] by accelerating the corrosion phenomenon. The differences between each accelerated corrosion technique and the natural corrosion process have been widely discussed in the literature [23, 26]. The imposed current technique is the most commonly used when studying the structural effect of steel reinforcement corrosion. However, many studies have shown that the choice of the current density value has a direct consequence on the similitude with natural corrosion. Especially, the crack patterns or the chemical nature of rust products is affected. However, most of the existing studies suggest not to exceed $100 \mu\text{A cm}^{-2}$ to have similar structural effects to natural corrosion [2, 27].

The imposed current technique consists in applying an electrical current from a Direct Current (DC) power supply between the cathode, which is a stainless steel grid, and the anode, which is the reinforcement inside the RC specimen [27]. The whole specimen is immersed in an electrolytic solution containing chlorides in order to ensure electrical conduction and to be representative of corrosion by chlorides.

One of the objectives of this study is to separately assess the effect of corrosion of the different reinforcement parts (longitudinal and transversal reinforcements) on the mechanical response of the specimens. For this reason, three beam configurations are considered:

- C_1 for the longitudinal reinforcement corrosion;
- C_2 for the stirrups corrosion;
- C_3 for the full reinforcement corrosion.

In order to reach the corrosion targets for the three configurations, different parts of reinforcement were electrically insulated and different cathode settings were adopted, depending on the configuration.

As recommended in [28], the current density was limited to $100 \mu\text{A.cm}^{-2}$ in order to obtain rust products as similar as possible to those formed in natural conditions. Despite the fact that the chemical nature of rust product is not strictly equivalent to the one observed in case of natural corrosion, the mechanical consequences of rust formation are the same [29].

Three corrosion rates, expressed in terms of mass losses are targeted:

- 5%, because many studies demonstrated a degradation of the bond between steel and concrete for a corrosion rate between 1.5% [30] and 5% [3, 31];
- 10%, rate from which civil engineering maintenance operations start [32];
- 15%, demonstrated in some studies to be the threshold from which a change of the steel failure mechanism is observed [1, 33].

All the RC beams are immersed in a 3.5% NaCl solution. The exposure time is estimated for each type of beam and each corrosion rate using Faraday's law (Eq. 1) with $\alpha = 1.3$ [5]. The required exposure duration varies from 31 to 141 days, depending on the targeted corrosion rate and on the beam configuration.

$$\Delta t = \frac{\alpha \cdot \Delta w \cdot z \cdot F}{M \cdot I} \quad (1)$$

In Eq. (1), Δw is the mass of steel consumed due to corrosion ($\text{kg} \cdot \text{m}^{-2}$), I is the current density ($\text{A} \cdot \text{m}^{-2}$), Δt is the exposure time (s), F is the Faraday constant $96\,500 \text{ (C} \cdot \text{mol}^{-1}\text{)}$, z is the ionic charge (2 for Fe), M is the atomic weight of steel ($\text{g} \cdot \text{mol}^{-1}$), α is a coefficient usually taken between 1 and 2 to take into account the duration of chloride ingress into concrete before reaching the rebar.

Since the actual corrosion degree is difficult to measure experimentally on the tested beams due to their large dimensions as well as the high reinforcement density, 9 dedicated RC specimens were cast. The same concrete formulation and steel reinforcement as the real tested beams are used. The specimens were corroded at 5, 10 and 15% using the same setup previously described. The rebars were removed from the concrete and mechanically cleaned afterwards. Table 1 summarizes the mean weighing results.

Table 1 Mean weighting results

Target corrosion rate (%)	Measured corrosion rate (%)
5	3.1
10	6.3
15	9.4

Since the chloride RC corrosion is not uniform, the mass loss ratio is not a sufficient indicator to characterize the corrosion state. For this reason, using the same bars dedicated to the mass loss measurement, the distribution of the steel cross section diameter has been measured. The measurements have been realized by the means of a profilometer bench with a running transverse laser beam along the bar.

As long as the bending behavior is studied in this experimental campaign, only the longitudinal rebars are inspected. Table 2 summarizes statistical indicators coming from the measured diameter distributions.

For the sake of clarity, each beam is labeled hereafter with respect to its corrosion configuration (C_1, C_2 , or C_3) followed by the targeted corrosion rate (5, 10 or 15%). To be more specific, the label C_n_R refers to the configuration n and to the corrosion rate R . For example, the label $C1_{15}$ corresponds to a longitudinal corrosion beam corroded at 15%.

2.4 Experimental setup and test program

Experimental testing consists of a quasi-static as well as a dynamic characterization. 9 corroded specimens (3 corrosion rates and 3 corrosion configurations) and a unique reference beam are tested by means of the strong floor. The dynamic testing of the 9 other corroded beams (3 corrosion rates and 3 corrosion configurations) in addition to another virgin beam is performed on the AZALEE shaking table. The setup is similar to the one used for the IDEFIX campaign [17]. Some modifications have been made to adapt the experimental setup for accommodating high range displacements and rotations.

The beams are excited for both dynamic and quasi-static tests along their weakest flexural axis; the boundary conditions are the followings:

- rotating supports allowing the rotation at the beam extremities around the vertical axis. These supports are designed to ensure a maximum rotation angle of $\pm 24^\circ$ at the beam boundaries. This choice is consistent with the expected maximal displacement imposed at the loading points of $\pm 400 \text{ mm}$;
- two additional masses, of 94 kg weight each, fixed at the intermediate supports. These masses ensure a first natural frequency of the beams in the range of 12 and 13 Hz. The total mass of each intermediate



Table 2 Statistical indicators of the measured diameter distributions

Targeted mass loss (%)	Minimum diameter (mm)	Maximum diameter (mm)	The average diameter (mm)	Standard deviation (mm)
0	11.693	13.555	12.096	0.144
5	10.901	12.598	12.083	0.167
10	9.820	12.983	11.997	0.300
15	9.656	12.766	11.797	0.295

support including the two additional masses is around 310 kg;

- two air-cushion systems to bear the beam weight and to drastically reduce the friction between the beam and the shaking table's or strong floor's upper plate. These measures are taken to prevent the beam from cracking under the addition of its self-weight and the lumped masses weight.

2.4.1 Quasi-static testing

Regarding the quasi-static tests, the corroded and non-corroded beams are subjected to a classical four-point reverse cyclic bending test on the TAMARIS strong floor. The loading is applied by means of a long-stroke actuator. This actuator is linked with a reinforced metal beam able, through swivels at its ends, to distribute the loading on two points of the DYSBAC beam. The actuator of 100KN capacity has a maximum displacement of $\pm 500\text{mm}$ and a maximum velocity of $1.7\text{m}\cdot\text{s}^{-1}$. A general view on the experimental setup is shown in Fig. 1. The choice of four-point rather than three-point bending test is justified by the desire to have a distributed instead of a localized damage. This choice does not necessarily constrain the beam failure to occur at midspan.

The applied loading is composed of blocks of three identical cycles during which the displacement is controlled, with an increasing amplitude between two consecutive blocks (Fig. 2). The displacement speed is controlled at 0.5 mm/s. Each cycle involves 4 phases: loading in one direction, unloading, loading in the other direction and unloading. Unloading is performed up to recovering a zero force measured with the actuator load cell. The goal of this loading protocol is to have 3 identical cycles to stabilize the new damage level associated with the current block before moving

on to the next one. The amplitude range varies from 0.4 mm up to 200 mm.

Hammer shock tests are also performed between the blocks in order to get the evolution of the modal properties with damage. Two impact positions are considered: at midspan and near an intermediate support. The modal properties presented in this paper are the mean values of the modal properties determined with each hammer test using the measured acceleration at the different sensors positions. In order to decrease the intrinsic discrepancy related to these tests, they have been performed by the same operator all along the experimental campaign.

2.4.2 Dynamic testing

The dynamic tests are performed on the AZALEE shaking table. It is a $6 \times 6\text{m}^2$ shaking table able to reproduce seismic signals up to $3g$ depending on the payload. The table is controlled on the 6 degrees of freedom (3 rotations, 3 translations) (Fig. 3).

The dynamic loading consists in a synthetic signal able to excite only the first natural mode of the beam. This bandlimited signal has been chosen in order to have a quasi-constant power spectral density over the entire frequency domain of interest [2 Hz, 13 Hz] (according to the displacement limits of the shaking table). This choice has been made in order to take into account the frequency shift due to the damage growth during the test. 5 peak acceleration levels are used: 0.125g, 0.5g, 0.8g, 1.25g and 2g. A modal characterization of each beam is performed before testing and between two consecutive testing sequences using a white noise (WN) signal ($PGA = 0.1g$).

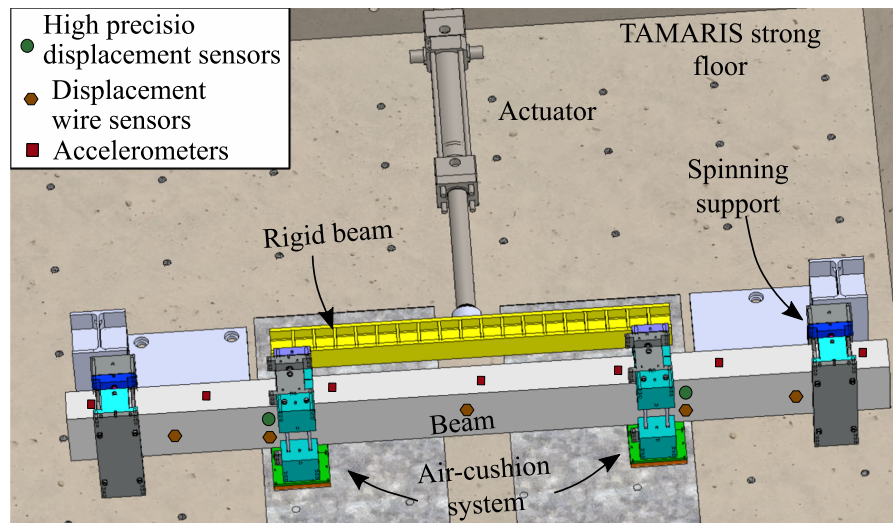


Fig. 1 General view of the experimental setup for the quasi-static tests

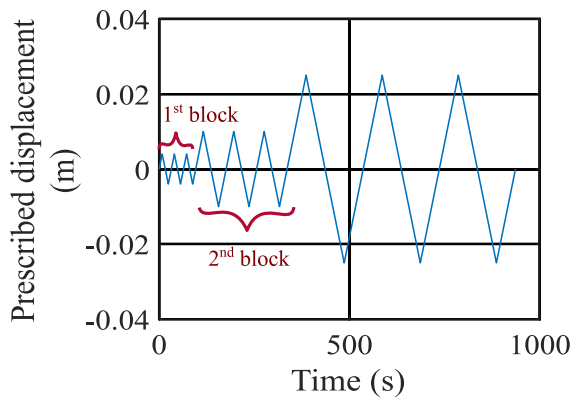


Fig. 2 Applied loading in quasi-static testing

2.4.3 Measurements

In order to fully characterize the mechanical response of the specimens during the tests, different types of sensors are used:

- 5 displacement wire sensors;
- 2 high precision displacement wire sensors;
- 2 six-axis load cells at the beam ends;
- 7 three-axis accelerometers;
- Actuator load cell.

In addition, the digital image correlation (DIC) technique is used. It consists of black and white strips

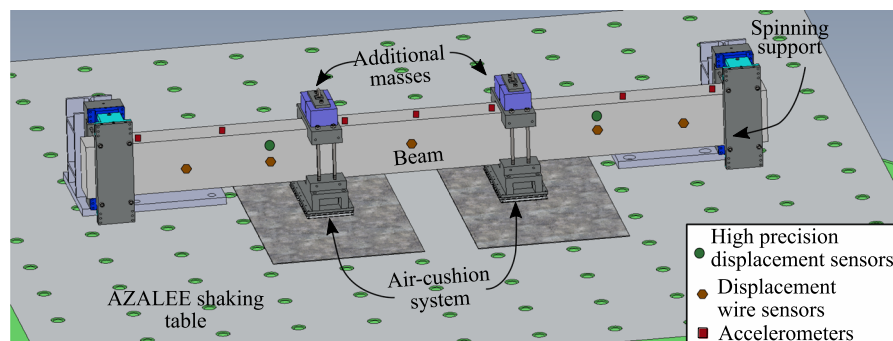


Fig. 3 General view of the experimental setup for dynamic tests

printed all along the upper surface of the beam. The whole beam is filmed from above using a stereovision

rig. In this way, the deformed shape of the beam during the tests can be post processed after testing.

3 The damping capability identification

The equivalent damping is an interesting feature to study when assessing the seismic behavior of RC structures. It measures the capability of a structure to dissipate the input energy. This parameter depends on the structure's ductility demand as well as on the plastic hinges position [34]. The EVDR (ξ_{eq}) is calculated as the sum of an elastic damping ξ_{elas} and an hysteretic one ξ_{hyst} [35] (see Eq. 2).

$$\xi_{eq} = \xi_{elas} + \xi_{hyst} \quad (2)$$

ξ_{elas} accounts for the damping when the RC element remains in the elastic domain. It is commonly taken equal to 2% [36]. ξ_{hyst} accounts for the damping induced by hysteretic phenomena.

In a predictive numerical context, the EVDR is calibrated in order to dissipate the right amount of energy by a viscous force field, acting proportionally to the velocity field. However, a more classical approach consists of assigning a damping ratio value to each eigenmode of the structure.

In this part, several identification methods are used to estimate the specimens damping. These methods can be divided into two categories:

- Methods using the structure response subjected to low level loads (hammer shock excitation or low level white noise signal). The identification of the modal properties using low level loads is of primary importance when dealing with dynamic monitoring of existing structures. In this study, the covariance-driven stochastic subspace identification (SSI) method [37] is used for both hammer shock and white noise tests. The main objective is to compare the trends revealed by both types of testing;
- Methods based on the structure response subjected to high level loads (quasi-static or dynamic). This type of identification methods is useful for numerical model calibration. For quasi-static loads, Jacobsen's area method [13] is used to evaluate dissipated and stored energy and therefore the equivalent viscous damping ratio. For dynamic loads, the non-parametric identification method

[17] applied on the structure displacement response can provide a valuable information about the evolution of modal properties (natural frequency and damping ratio) along time depending on the damage sustained by the structure along the loading.

Since the specimen exhibits a behavior that mostly includes bending and only the first eigenmode of the beam is excited during the dynamic testing, the focus is made on 1st natural mode exclusively. However, the acquired data allow a similar analysis for the 2nd eigenmode which can be performed if needed.

It is to be noted that the C3_15% beam is excluded from the results discussion. This is due to an incident that occurred during the corrosion process.

3.1 Covariance-driven stochastic subspace identification method

The experimental modal analysis is a powerful tool for describing, understanding and modeling the dynamic behavior of a structure. It consists of determining the natural frequencies, mode shapes and modal damping ratios based on the measured experimental data.

The covariance-driven stochastic subspace identification (SSI) method is an effective instrument for the experimental modal identification driven by output-only records [38–40]. It is of a great interest when the input information is unknown (e.g., traffic load or wind load). Thus, the excitation is assumed to be a realization of a stochastic process. In [37], a detailed overview on the covariance-driven SSI method basic theory is given.

3.1.1 Quasi-static testing condition

Thanks to the hammer shock tests performed during the quasi-static campaign after each loading block, the modal damping ratio can be identified. The objective of such characterization is to assess the evolution of the damping capability as a function of the damage level experienced by the structure. In addition, the influence of the corrosion ratio on the damping capability is investigated. The covariance-driven SSI method is used (see Sect. 3.1) to identify the corresponding modal damping ratio for each RC beam subjected to hammer shock tests.

Table 3 Natural damping ratio of the specimens before loading based on hammer shock modal testing

Configuration	Reference	C ₁			C ₂			C ₃	
		5	10	15	5	10	15	5	10
Corrosion ratio (%)	0								
1st natural frequency (Hz)	12.31	12.33	12.72	12.45	12.35	12.40	12.38	12.12	12.42
1st modal damping ratio (%)	2.5	2.7	3.4	3.4	2.7	2.6	2.7	2.5	4.2

Table 3 summarizes the 1st natural frequency as well as the 1st damping ratio of each specimen prior to any load testing. Regarding the effect of corrosion on the 1st natural frequency, no particular trend could be noted. It is generally known that natural frequencies have low sensitivity to damage [41, 42].

On the contrary, an increase in the 1st damping ratio is basically observed as the corrosion level gets higher, especially for the C₁ and C₃ configuration beams. This observation is consistent with a previous study reported in the literature [14].

However, another previous study dealing with the effect of general corrosion on the modal properties of RC elements, has shown an opposite trend of the 1st damping ratio [15]. The inconsistency between the two studies may be explained by the fact that the corrosion degradation type is different, leading to non-similar structural effects. In the present study, the localized corrosion induces a local loss of bond strength, which is not the case for generalized corrosion where the degradation is more global. In generalized corrosion, the steel cross-section loss is uniform and thus remains small even if the total corrosion ratio is high. In contrast, the localized corrosion is characterized by a sharp local reduction in the rebar cross-section. The coupling between these two effects of localized corrosion, which are the localized bond strength loss and the localized corrosion pits, is studied in [43].

Figure 4 depicts the relationship between the 1st modal damping ratio and the ductility level for each beam configuration and corrosion rate. To quantify the ductility level, the following index is introduced:

$$\mu = \frac{\max|u(t)|}{u_y} \quad (3)$$

where $\max|u(t)|$ is the maximum of the absolute value of the relative displacement measured at midspan with respect to the supports during the loading block prior

to the hammer shock test, and u_y is the midspan displacement corresponding to the first yield occurrence in the steel rebars for the concerned beam.

The procedure adopted in this work for the evaluation of u_y is the Park's method [44]. First, it consists of computing both secant and post-yield stiffness, and second determining their intersection points. The yield displacement is computed as the average of the two values obtained at the intersecting points. The main advantage of this method is the possibility to take into account the asymmetries observed in the two loading directions.

For the C₁ configuration, the corroded beams exhibit a smaller damping capability compared to the reference beam, as shown in Fig. 4a. In particular, when the steel yielding occurs, which corresponds to a ductility level equal to 1, the 1st damping ratio decreases with an increasing corrosion degree. This trend can be explained by the fact that the bonding between steel and concrete is enhanced for lightly corroded specimens [3].

In Fig. 4b, it can be noticed that C₂ corroded beams curves give similar trend regarding the 1st modal damping ratio evolution, regardless of the degree of corrosion. Moreover, a drop-off in the damping capability is observed at each ductility level for each corroded beam compared to the virgin one.

It can be noticed that the stirrups corrosion induces the highest damping decrease compared to the other corrosion configurations. Furthermore, the similarity between the values of the 1st modal damping ratio for each C₂ beam at each ductility level confirms that for low corrosion ratios the bond between steel and concrete is enhanced [3, 45].

Regarding the C₃ corroded beams, a decrease in the 1st modal damping ratio is observed for the C3_5%, C3_10% at each ductility level after yielding. It is important to note that for the C₃ corroded beams, the corrosion process using the imposed current induces a

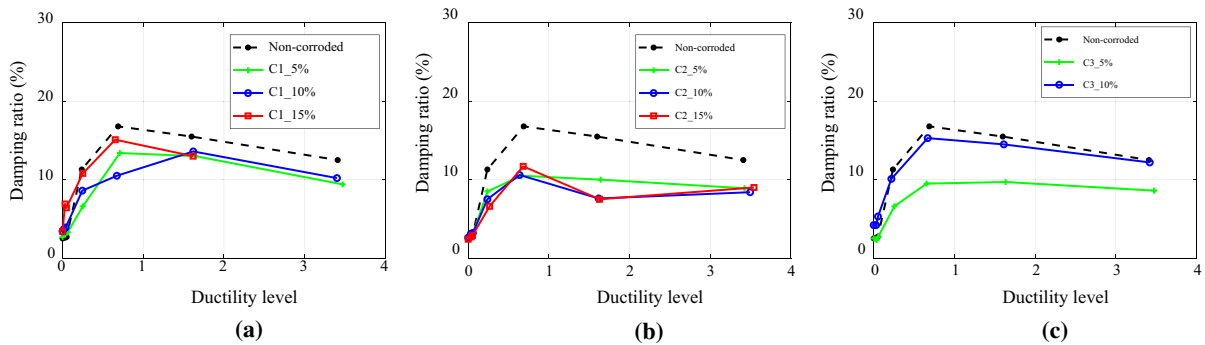


Fig. 4 Evolution of first damping ratio obtained from hammer shock tests: **a** C₁ configuration, **b** C₂ configuration, **c** C₃ configuration

heterogeneous corrosion state at the longitudinal reinforcement and stirrups level. This is because only one DC power supply is used. Therefore, the distribution of the electrical current depends on the resistivity of the different reinforcement parts. Based on the values displayed in Fig. 4c, it could be conjectured that for C₃_{10%} beam the mainly corroded part is the longitudinal rebars, whereas it is stirrups for C₃_{5%} beam.

For all the tested beams, a change in the shape of the curves is observed near the yielding point (ductility = 1). The 1st damping ratio increases first, then slightly decreases in the vicinity of the yielding point till the loading ends. This observation is in good agreement with the fact that the modal damping ratio increases with an increasing crack depth, as demonstrated in [46].

3.1.2 Dynamic testing condition

During the dynamic campaign, the WN applied on each tested beam after each testing sequence made possible the identification of the modal properties using the covariance-driven SSI method introduced in Sect. 3.1. The objectives are the same as those targeted in Sect. 3.1.1.

The 1st natural frequency as well as 1st natural damping ratio identified with white noise modal testing of each beam before being damaged by the dynamic loading is presented Table 4. Based on these results, an increase in the modal damping ratio with an increasing corrosion degree is observed. These results are consistent with those issued from hammer shock tests in Sect. 3.1.1 and with a recent study reported in the literature [16]. As far as the 1st frequency is concerned, no specific effect of corrosion could be

observed. These results are consistent with those coming from hammer shock testing in Sect. 3.1.1.

The evolutions of the 1st damping ratios of each beam configuration and each corrosion rate, as a function of the ductility level are presented in Fig. 5. The ductility level is evaluated in the same way as for quasi-static testing according to Eq. 3. The maximum displacement involved in Eq. 3 is measured during the dynamic test performed before the concerned WN test. The computation of the yielding displacement was inspired from the Park's method [44] applied on the capacity curves issued from dynamic testing.

After the beams dynamic loading, an increase of the damping ratio with an increasing damage or ductility level is noticed [16]. Regarding the effect of the corrosion degree, the damping capability is reduced with an increasing corrosion degree especially for the C₂ beams. These observations are fully consistent with the quasi-static testing results.

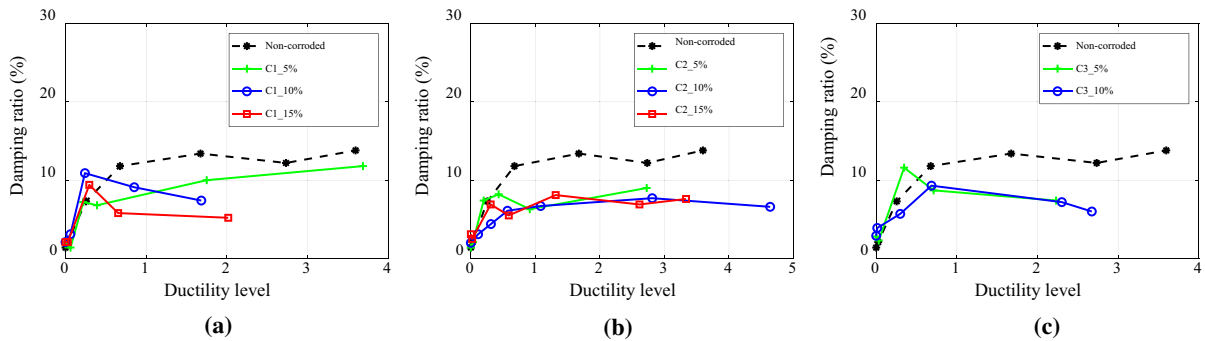
However, the results of the current study are not consistent with a study carried out on corroded RC bridge piers [16]. In the latter, an increase in the damping ratio at each ductility level with the increase of the corrosion degree is observed. The incoherence between the two studies may be due to the difference between the tested specimen (beam/column and corrosion along the beam/partial corrosion of the column) as well as the targeted corrosion degrees which are much higher (6 ~ 23% for longitudinal rebars and 10 ~ 46% for stirrups) [16].

4 Discussion

In this part, a comparison between the results exposed in Sects. 3.1.1 and 3.1.2 is carried out. This

Table 4 Natural damping ratio of the specimens before loading based on white noise modal testing

Configuration	Reference	C ₁			C ₂			C ₃	
		5	10	15	5	10	15	5	10
Corrosion ratio (%)	0								
1st natural frequency (Hz)	12.21	12.34	12.69	12.01	12.30	11.92	12.03	12.32	12.151
1st modal damping ratio (%)	1.4	1.8	2.1	2.1	1.4	2	3.1	2.8	2.9

**Fig. 5** Evolution of first damping ratio obtained from dynamic tests: **a** C₁ configuration, **b** C₂ configuration, **c** C₃ configuration

comparison is relevant since the same experimental setup was used for both quasi-static and dynamic testing and the modal damping ratio was computed based on the same identification method.

Prior to load testing, we can observe an increase in the modal damping ratio with an increasing corrosion degree. This conclusion is drawn by both quasi-static [14] and dynamic testing [16].

When the beams are loaded, both types of testing confirm the increase of the damping capability with an increasing damage level seen in [46].

Regarding the values of the 1st modal damping ratios measured on the basis of quasi-static and dynamic tests, a slight difference is observed for a given beam at a given ductility level. This discrepancy may be explained by the fact that the injected energy during a hammer shock is not similar to the one injected during a WN signal.

The difference between the two levels of energy is both quantitative and qualitative. Not the same amount of energy is injected in the system during hammer shock or WN tests. In addition, the hammer shock testing imposes an impact force on the beam, whereas the WN signal leads to a distributed force that acts on the entire beam.

4.1 Jacobsen's areas method

4.1.1 Method

Jacobsen [13] suggested a method to estimate the EVDR. This method is applicable for a single degree of freedom (SDOF) oscillator excited by mono-harmonic force. The EVDR is calculated according to Eq. 4.

$$\xi_{eq} = \frac{1}{4\pi} \cdot \frac{\omega_0}{\omega} \cdot \frac{E_d}{E_s} \quad (4)$$

where E_d is the dissipated energy during a cycle, E_s is the stored elastic potential energy, ω is the excitation frequency and ω_0 is the eigenfrequency of the oscillator.

In a displacement-force diagram, the dissipated energy E_d is calculated as the area enclosed in the loop. Whereas, the stored energy E_s is computed by different methods based on the particularity of the tested elements [47, 48, 10, 11].

For both quasi-static and dynamic loading, asymmetries can be observed. For this reason, specific methods [47, 48] derived from the former Jacobsen's area method are used to take into account these

asymmetries in the computation of dissipated and stored energy.

Figure 6 is a representation of the dissipated and stored energy involved in the calculation of EVDR in this paper. The plotted displacement-force diagram corresponds to the response of the reference beam subjected to a cycle of 5 cm amplitude.

Since the EVDR depends on the excitation frequency ω and the eigenfrequency ω_0 , the use of Jacobsen's area method in quasi-static testing needs to be justified. For this reason, the deformed shape of DYSBAC specimen subjected to 4 point-bending test as well as the 1st mode shape are calculated relying on the models shown in Fig. 7.

As depicted in Fig. 8, the beam deformed shape under four point bending test and the beam 1st mode shape are similar. The local error between the two shapes (see Eq. 5) does not exceed 3%.

$$\varepsilon_{err}(x) = \frac{u(x) - \phi(x)}{\phi(x)} \quad (5)$$

where x is the position along the beam, u is deformed shape and ϕ is the 1st modeshape.

The normalized experimentally measured displacement by the DIC technique is also shown in Fig. 8. a, for the reference beam at 0.8 mm imposed displacement. The differences noted between the theoretical and the experimental deformed shapes is due to the quality of the measurement itself (see Sect. 2.4.3), the concrete cracking even in early stages of loading as well as the backlashes presence in the experimental assembly.

Since the calculated local error between the two shapes is less than 3%, we can assume that the beam subjected to the four point bending test deforms as a

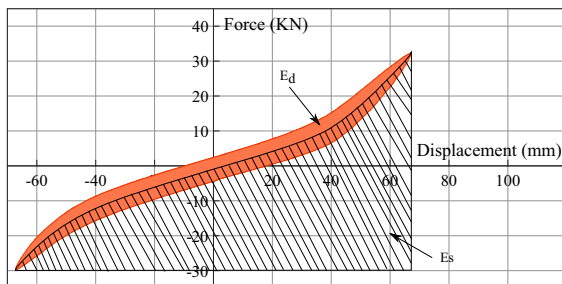


Fig. 6 Jacobsen's areas method applied to the virgin beam response subjected to a 5 cm amplitude cycle

SDOF oscillator excited by a mono-harmonic force with $\omega = \omega_0$.

4.1.2 Dissipated energy

Based on quasi-static tests, the dissipated energy is evaluated for each beam and for each loading block. Based on the beam response to a given loading block, the area of the third cycle, where the damage is assumed to be stabilized, is computed. It should be noted that only loading blocks with an amplitude higher or equal to 4 mm have been considered in this part. This is because the measurement uncertainty is high for low imposed displacements. This may be explained by the precision of the measurement system itself as well as the unavoidable presence of backlashes in the experimental setup.

Figure 9 illustrates the evolution of the dissipated energy as a function of the ductility level for each tested beam. For all the tested beams, the dissipated energy increases with an increasing ductility level. This is due to the increase of damage level due to the concrete cracking and thus the dissipation capability. This observation is in a good agreement with the results reported in previous studies [46].

It is also observed that an increasing corrosion degree leads to a decrease in the dissipation capability, as shown in Fig. 9. These results are consistent with the previous studies [10, 11] that showed that the corroded RC elements are characterized by a low hysteretic response and a reduced dissipation capability.

Regarding the difference between each beam configuration dissipation capability, no major differences could be observed between two different beam configurations corroded at the same degree.

4.1.3 Stored energy

The elastic stored energy is evaluated according to the method exposed in Sect. 3.2.1 for each tested beam at each loading level. Figure 10 shows the stored energy evolution as a function of ductility level for each tested beam.

Based on the curves obtained, no major differences could be observed between the different tested beams as far as the elastic stored energy is concerned. These results are not consistent with those observed in [10]. The experimental study carried out on corroded bridge

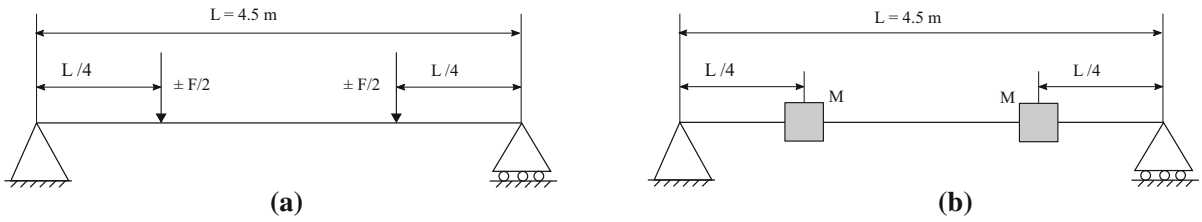


Fig. 7 DYSBAC beam modeling: **a** Quasi-static, **b** Dynamic

Fig. 8 Comparison between the computed deformed shape under four point bending test and 1st modeshape: **a** Normalized displacement, **b** Local error

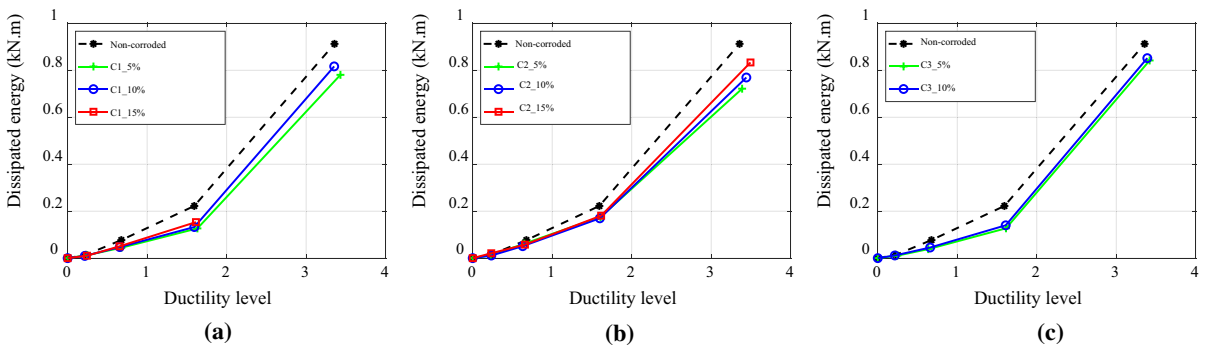
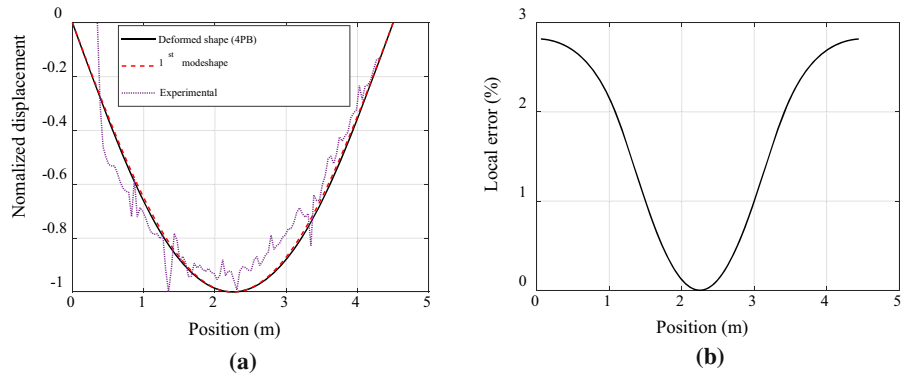


Fig. 9 Evolution of the dissipated energy: **a** C_1 configuration, **b** C_2 configuration, **c** C_3 configuration

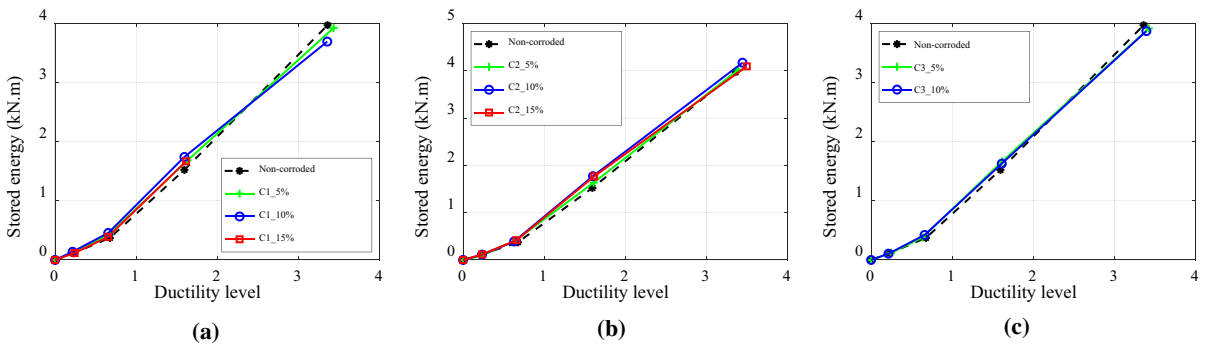


Fig. 10 Evolution of the stored energy: **a** C_1 configuration, **b** C_2 configuration, **c** C_3 configuration



piers showed a decrease in the stored elastic energy as the severity of corrosion gets worse.

The discrepancy between the results of the current study and the conclusions drawn by [10] may be explained by the difference of the considered specimens in addition to the boundary and loading conditions. In [10], the specimens are cantilever columns fixed to the building rigid foundation, loaded by a constant vertical force and subjected to a cyclic horizontal loads. These settings affect the storing energy capability of the specimen as well as the appearance of plastic hinges [49].

4.2 EVDR

The EVDR has been evaluated according to the Jacobsen's area method for each tested beam at each loading level. The curves describing the evolution the EVDR as a function of the ductility level are shown in Fig. 11.

A decrease in the EVDR for the corroded specimens in comparison with the reference beam is observed. As exposed in Sect. 3.1.1, the steel/concrete bonding enhancement in the case of slightly corroded structures can explain this conclusion. The obtained results are also in a good agreement with the conclusions drawn by [11].

4.3 Non-parametric identification

In this part, the beam responses to high level dynamic loads are investigated. The non-parametric identification method is used to determine the evolution of natural frequency and the damping ratio over the testing time. This identification strategy is suggested in [17] and was applied on the response of RC beams

subjected to an intermediate and high level WN signal on the shaking table.

The main advantage of this method is that no surrogate model has to be assumed in order to identify the modal properties evolution. The displacement field coming from DIC technique (see Sect. 2.4.3) is projected on the analytical modal basis computed by the beam theory. The modal basis can be truncated or enriched to represent the nonlinearities occurring during the dynamic tests.

Time is divided into time windows. For each time window and each eigenmode i , the i th SDOF oscillator response, subjected to the i th modal force, is computed for a set of parameters (i th eigenfrequency, i th modal damping ratio), according to the Newmark method [50]. Subsequently, the resulting displacement is compared to the modal experimental displacement. An optimization algorithm is used to determine the modal properties (i th eigenfrequency, i th modal damping ratio) for each time-window and the modal displacement for each considered eigenmode. This algorithm is based on the minimization of an error function between the projected experimental displacement and the i th computed displacement.

The modal displacements are combined to reconstruct an approximate displacement field afterwards. An illustration of the algorithm output results is presented in Fig. 12. This example corresponds to the reference beam subjected to an acceleration level of $0.5g$.

The choice of the time window size has a considerable effect on the results quality [17]. Therefore, rather than choosing a constant time window size [17], in the current study a variable window time size is considered. The size of each time window depends on the previous time window resulting eigenfrequency. It

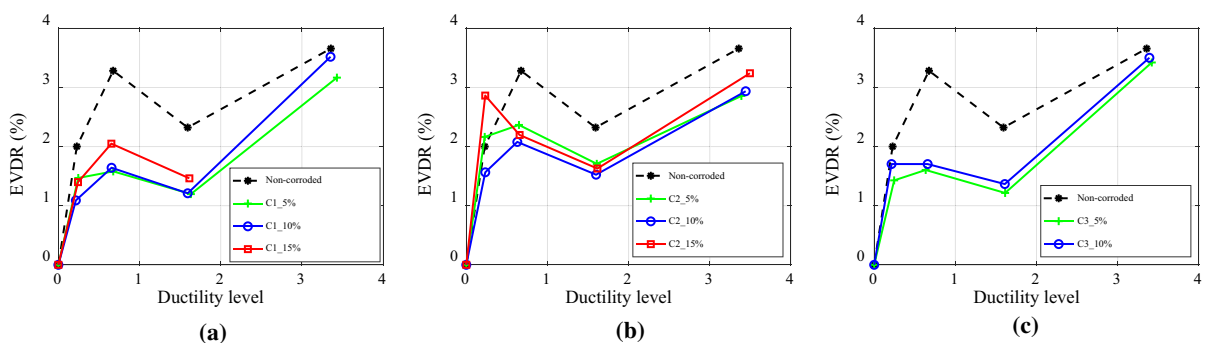


Fig. 11 Evolution of the EVDR: **a** C₁ configuration, **b** C₂ configuration, **c** C₃ configuration

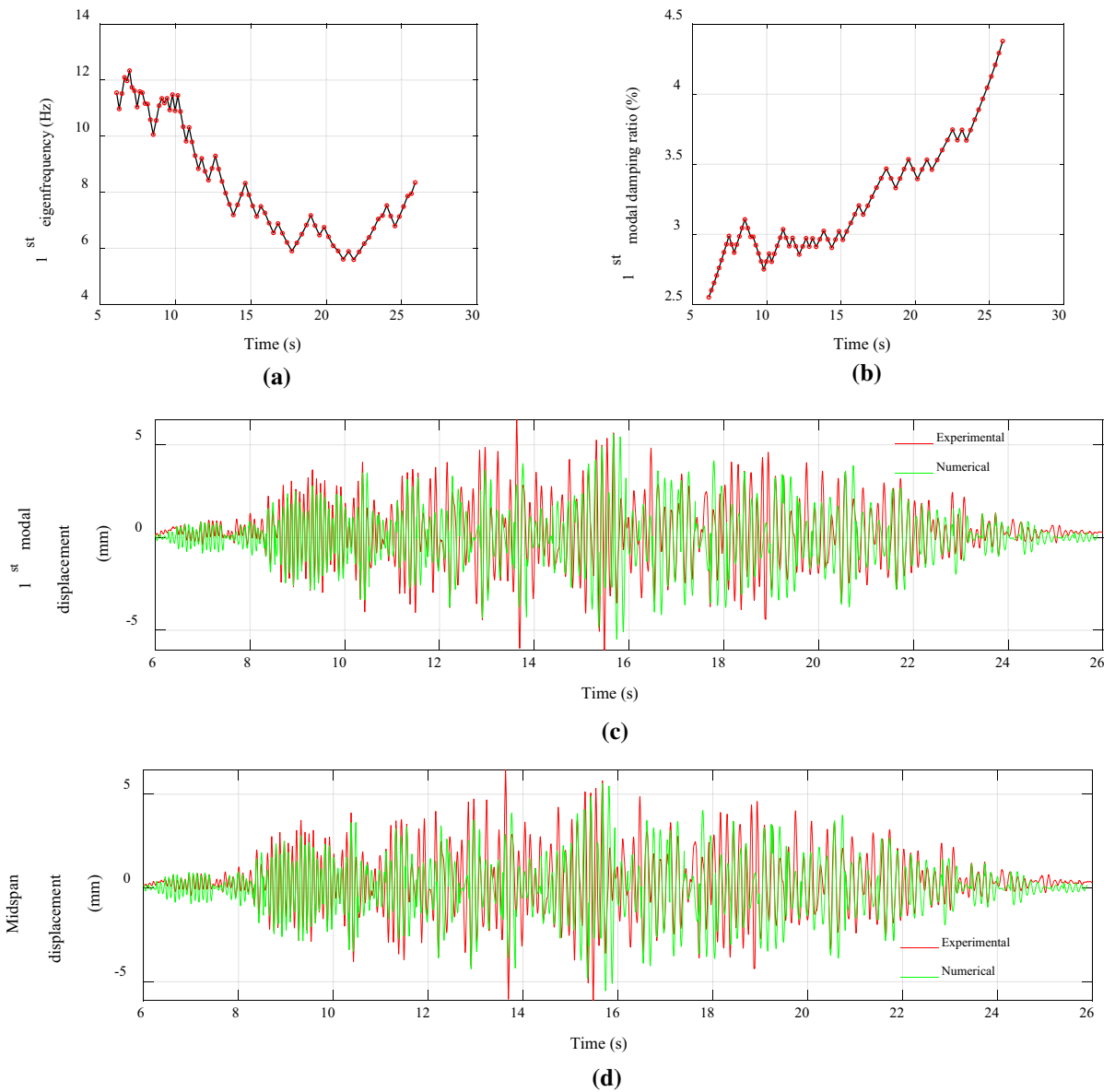


Fig. 12 Example of the algorithm output results for the reference beam at 0.5 g acceleration level: **a** the 1st eigenfrequency evolution, **b** the 1st modal damping ratio evolution, **c** the 1st modal displacement evolution, **d** the midspar displacement evolution

should include two periods of the previously computed SDOF oscillator (see Eq. 7).

$$\begin{cases} L_0 = 0.3s \\ L_i = \frac{2}{f_{i-1}} \end{cases} \quad (7)$$

where L_0 is the initial time window size, L_i is the size of the current time window and f_{i-1} the 1st

eigenfrequency of the computed SDOF oscillator in the previous time window.

Since the final result, which is the approximate displacement field, is the combination of the different approximate modal displacements, the size of each time window is determined using the 1st natural frequency. The so-computed size of the successive time windows is then kept for the other eigenmodes. In the present study, a good match between the numerical



and experimental displacement field could be found by considering only the first two eigenmodes.

From Fig. 12a, in a first phase a decrease in the 1st natural frequency along with time is observed. This result can be explained by the cracks development and the damage growth due to the seismic loading. A second phase where the natural frequency increases over time follows. This is indicative of the crack closure and the gain in stiffness due to the decrease of the excitation level at the end of each testing sequence. The shape of the curves is found for all the tested beams at each acceleration level.

The evolution of the 1st modal damping ratio over time has been determined using the non-parametric identification method for each tested beam. Four accelerations levels have been considered for all the beams: 0.125g, 0.5g, 0.8g and 1.25g.

Figure 13 shows the evolution of the mean 1st modal damping ratio at each considered acceleration level as a function of the ductility level.

From the second acceleration level (2nd point in each curve), it can be observed that, the general trend is an increase of the modal damping ratio as the damage level increases for all the tested specimens. This finding is similar to the results mentioned in part 3.1. The high mean damping ratio for 0.125g acceleration level is explained by the limited quality of the displacement field measurement. At this acceleration level, the measured displacement is in the range of 0 – 1mm, which made difficult the displacement field acquisition with a good precision.

Regarding the effect of the reinforcement corrosion on the modal damping ratio, no particular trend could be discerned using this specific identification method. It is probably due to the choice made of the average value as a representative parameter of the damping

ratio time evolution. Given the fact that the mean values smooth out the local variability, which is predominant in our case of study. However, it should be noticed that the advantage of this method is the evaluation of the modal damping during a seismic loading. These identified values are different from those identified from a hammer shock or a WN testing. This is mainly because the injected energy in the system during a seismic sequence is higher than the injected energy during the modal analysis testing.

5 Conclusions

In this paper, an extensive experimental campaign aiming at assessing the influence of corrosion on the dissipation capability of RC components has been detailed. 18 corroded beams and 2 additional reference beams have been subjected to quasi-static and dynamic testing using the same experimental setup.

The main results can be summed up as follows:

- When the specimens are unloaded, an increase in the modal damping ratio with an increasing corrosion degree is observed. The same conclusion can be drawn based on both quasi-static and dynamic testing;
- When the specimens are loaded, either by quasi-static or dynamic loading, the modal damping ratio measured on corroded specimens decreases as the corrosion severity becomes worse;
- The modal damping ratio increases with an increasing damage level for all the tested beams. This conclusion is confirmed by quasi-static and dynamic and quasi-static tests;

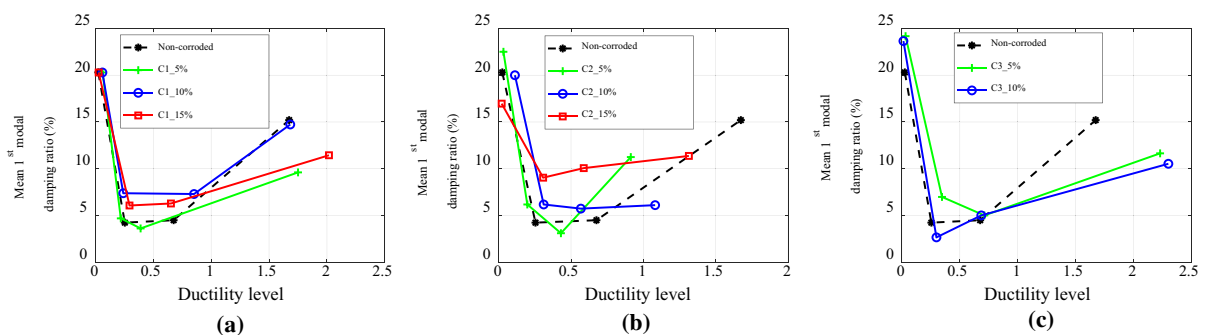


Fig. 13 Evolution of the 1st modal damping ratio: **a** C₁ configuration, **b** C₂ configuration, **c** C₃ configuration

- The modal damping ratios have been computed using the same identification method on the results issued from both hammer shock and WN tests. A slight difference in the damping ratio values is noticed. This is mainly due to the difference between the two considered excitations (local/distributed);
- For the quasi-static tests, the dissipated energy and the equivalent viscous damping ratio decrease with an increasing corrosion degree;
- For the dynamic tests, the non-parametric identification method was applied. The effect of the corrosion on the average value of the modal damping ratio evolution during a test sequence could not be discerned. However, it should be noticed that this method made possible the identification of the modal damping ratio evolution during the seismic sequence. The obtained values are different from the modal damping ratios coming from the modal analysis tests;
- the covariance-driven SSI method gives consistent results for hammer shock and white noise tests. Jacobsen's area method applied on quasi-static cyclic responses, gives the same trends as revealed by the hammer shock and white noise characterization. The non-parametric identification method reveals the high variability of the damping ratio of the tested specimens during a given seismic sequence. Hence, this identification method seems to be the most suitable to identify a non-linear model.

As a major outlook of the present study, a simplified numerical model being able to take into account the different effects of corrosion at the material scale is under development. The main objective of this simplified model is to reproduce the different structural consequences observed by this experimental campaign [51].

Acknowledgements The French Institute for Radioprotection and Nuclear Safety (IRSN) and the Nuclear Energy Division of the French Sustainable Energies and Atomic Energy Commission (CEA/DEN) are kindly thanked for financial supports.

References

1. Almusallam AA (2001) Effect of degree of corrosion on the properties of reinforcing steel bars. *Construct Build Mater*. [https://doi.org/10.1016/S0950-0618\(01\)00009-5](https://doi.org/10.1016/S0950-0618(01)00009-5)
2. Andrade C, Alonso C, Molina FJ (1993) Cover cracking as a function of bar corrosion: Part I-Experimental test. *Mater Struct*. <https://doi.org/10.1007/BF02472805>
3. Almusallam AA, Al-Gahtani AS, Aziz AR (1996) Effect of reinforcement corrosion on bond strength. *Construct Build Mater* 10(2):123–129
4. Mancini G, Tondolo F, Iuliano L, Minetola P (2014) Local reinforcing bar damage in rc members due to accelerated corrosion and loading. *Construct Build Mater*. <https://doi.org/10.1016/j.conbuildmat.2014.07.011>
5. Meda A, Mostosi S, Rinaldi Z, Riva P (2014) Experimental evaluation of the corrosion influence on the cyclic behaviour of RC columns. *Eng Struct*. <https://doi.org/10.1016/j.engstruct.2014.06.043>
6. Malumbela G, Alexander M, Moyo P (2010) Variation of steel loss and its effect on the ultimate flexural capacity of RC beams corroded and repaired under load. *Construct Build Mater*. <https://doi.org/10.1016/j.conbuildmat.2009.11.012>
7. Malumbela G, Moyo P, Alexander M (2009) Behaviour of RC beams corroded under sustained service loads. *Construct Build Mater*. <https://doi.org/10.1016/j.conbuildmat.2009.06.005>
8. Rinaldi Z, Imperatore S, Valente C (2010) Experimental evaluation of the flexural behavior of corroded P/C beams. *Constru Build Mater*. <https://doi.org/10.1016/j.conbuildmat.2010.04.029>
9. Zhu W, François R (2014) Corrosion of the reinforcement and its influence on the residual structural performance of a 26-year-old corroded RC beam. *Construct Build Mater*. <https://doi.org/10.1016/j.conbuildmat.2013.11.015>
10. Guo A, Li H, Ba X, Guan X, Li H (2015) Experimental investigation on the cyclic performance of reinforced concrete piers with chloride-induced corrosion in marine environment. *Eng Struct*. <https://doi.org/10.1016/j.engstruct.2015.09.031>
11. Ma Y, Che Y, Gong J (2012) Behavior of corrosion damaged circular reinforced concrete columns under cyclic loading. *Construct Build Mater*. <https://doi.org/10.1016/j.conbuildmat.2011.11.002>
12. Casolo S, Milani G, Uva G, Alessandri C (2013) Comparative seismic vulnerability analysis on ten masonry towers in the coastal Po Valley in Italy. *Eng Struct* 49:465–490
13. Jacobsen LS (1960) Damping in composite structures, II WCEE, Tokyo
14. Zou DJ, Liu TJ, Qiao GF (2014) Experimental investigation on the dynamic properties of RC structures affected by the reinforcement corrosion. *Adv Struct Eng* 17(6):851–860
15. Razak HA, Choi FC (2001) The effect of corrosion on the natural frequency and modal damping of reinforced concrete beams. *Eng struct* 23(9):1126–1133
16. Yuan W, Guo A, Yuan W, Li H (2018) Shaking table tests of coastal bridge piers with different levels of corrosion damage caused by chloride penetration. *Construc Build Mater* 173:160–171



17. Heitz T, Le Maout A, Richard B, Giry C, Ragueneau F (2018) Dissipations in reinforced concrete components: Static and dynamic experimental identification strategy. *Eng Struct*. <https://doi.org/10.1016/j.engstruct.2018.02.065>
18. Mosley WH, Hulse R, Bungey JH (2012) Reinforced concrete design: to Eurocode 2. Macmillan International Higher Education, 2012
19. Fardis MN (2009) Seismic design, assessment and retrofitting of concrete buildings: based on EN-Eurocode 8, vol 8. Springer, Berlin
20. AFNOR (2005) Steel for the reinforcement of concrete – weldable reinforcing steel – General
21. Paradis F (2009) Influence de la fissuration du béton sur la corrosion des armatures : caractérisation des produits de corrosion formés dans le béton. Université Laval
22. Altoubat S, Maalej M, Shaikh FUA (2016) Laboratory Simulation of Corrosion Damage in Reinforced Concrete. *Int J Concret Struct Mater*. <https://doi.org/10.1007/s40069-016-0138-7>
23. Yuan Y, Ji Y, Shah SP (2007) Comparison of two accelerated corrosion techniques for concrete structures. *ACI Struct J* 104(3):344
24. Vidal T, Castel A, François R (2004) Analyzing crack width to predict corrosion in reinforced concrete. *Cement Concrete Res*. [https://doi.org/10.1016/S0008-8846\(03\)00246-1](https://doi.org/10.1016/S0008-8846(03)00246-1)
25. Xu J, Jiang L, Wang W, Jiang Y (2011) Influence of CaCl₂ and NaCl from different sources on chloride threshold value for the corrosion of steel reinforcement in concrete. *Construct Build Mater*. <https://doi.org/10.1016/j.conbuildmat.2010.07.023>
26. Ahmad S (2009) Techniques for inducing accelerated corrosion of steel in concrete. *Arab J Sci Eng* 34(2):95
27. El Maaddawy TA, Soudki KA (2003) Effectiveness of impressed current technique to simulate corrosion of steel reinforcement in concrete. *J Mater Civil Eng* 15(1):41–47
28. Caré S, Raharinaivo A (2007) Influence of impressed current on the initiation of damage in reinforced mortar due to corrosion of embedded steel. *Cement Concrete Res*. <https://doi.org/10.1016/j.cemconres.2007.08.022>
29. Ožbolt J, Sola E, Balabanić G (2015) Accelerated corrosion of steel reinforcement in concrete: experimental tests and numerical 3D FE analysis, in *CONCREEP 10*, 2015, p. 108–117
30. Coccia S, Imperatore S, Rinaldi Z (2016) Influence of corrosion on the bond strength of steel rebars in concrete. *Mater Struct* 49(1–2):537–551
31. Auyeung Y, Balaguru P, Chung L (2000) Bond behavior of corroded reinforcement bars. *Mater J* 97(2):214–220
32. Projet APPLETT : Durée de vie des ouvrages en béton : Approches prédictives performantielles et probabilistes, (2006)
33. Ouglova A (2004) Etude du comportement mécanique des structures en béton armé atteintes par la corrosion, PhD Thesis, Cachan, Ecole normale supérieure
34. Priestley MJN (1997) Displacement-based seismic assessment of reinforced concrete buildings. *J Earthquake Eng* 1(01):157–192
35. Smyrou E, Priestley MN, Carr AJ (2011) Modelling of elastic damping in nonlinear time-history analyses of cantilever RC walls. *Bulletin Earthquake Eng* 9(5):1559–1578
36. Richard B, Martinelli P, Voldoire F, Chaudat T, Abouri S, Bonfils N (2016) SMART 2008: Overview, synthesis and lessons learned from the International Benchmark. *Eng Struct* 106:166–178
37. Li Z, Fu J, Liang Q, Mao H, He Y (2019) Modal identification of civil structures via covariance-driven stochastic subspace method. *Math Biosci Eng* 16(5):5709–5728
38. Pappa RS, Juang JN (1988) Some experiences with the eigensystem realization algorithm
39. Van Overschee P, De Moor BL (2012) Subspace identification for linear systems: Theory—Implementation—Applications. Springer, Berlin
40. Liu K (1996) Modal parameter estimation using the state space method. *J Sound Vib* 197(4):387–402
41. Cao MS, Sha GG, Gao YF, Ostachowicz W (2017) Structural damage identification using damping: a compendium of uses and features. *Smart Mater Struct* 26(4):043001
42. Farrar CR, Jauregui DA (1998) Comparative study of damage identification algorithms applied to a bridge: I Experiment. *Smart Mater Struct* 7(5):704
43. Castel A, François R, Arliguie G (2000) Mechanical behaviour of corroded reinforced concrete beams—Part 2: Bond and notch effects. *Mater Struct*. <https://doi.org/10.1007/BF02480534>
44. Park R (1989) Evaluation of ductility of structures and structural assemblages from laboratory testing. *Bull N Z Soc Earthq Eng* 22(3):155–166
45. Li Q, Niu D, Xiao Q, Guan X, Chen S (2018) Experimental study on seismic behaviors of concrete columns confined by corroded stirrups and lateral strength prediction. *Construct Build Mater* 162:704–713
46. Panteliou SD, Chondros TG, Argyrakis VC, Dimarogonas AD (2001) Damping factor as an indicator of crack severity. *J Sound Vib* 241(2):235–245
47. Kumar SS, Krishna AM, Dey A (2015) Cyclic response of sand using stress controlled cyclic triaxial tests
48. Heitz T, Giry C, Richard B, Ragueneau F (2019) Identification of an equivalent viscous damping function depending on engineering demand parameters. *Eng Struct* 188:637–649
49. Crambuer R (2013) Contribution à l'identification de l'amortissement: approches expérimentales et numériques
50. Newmark NM (1959) A method of computation for structural dynamics. *J Eng Mech Div* 85(3):67–94
51. Lejouad C, Capdevielle S, Richard B, Ragueneau F (2019) A numerical model to predict the effect of corrosion on the dynamic behavior of reinforced concrete beams

